Automated detection method of thoracic aorta calcification from non-contrast CT images using mediastinal anatomical label map

Hidenobu Suzuki [a], Yoshiki Kawata [a],
Toshihiko Sugiura [b], Nobuhiro Tanabe [b], Yuji Matsumoto [c], Takaaki Tsuchida [c],
Masahiko Kusumoto [d], Kazuyoshi Marumo [e], Masahiro Kaneko [e], Noboru Niki [f]

[a] Institute of Post-LED Photonics, Tokushima University, Tokushima, Japan; [b] Department of Respirology, Chiba University, Chiba, Japan; [c] Department of Endoscopy, National Cancer Center Hospital, Tokyo, Japan; [d] Department of Diagnostic Radiology, National Cancer Center Hospital, Tokyo, Japan; [e] Tokyo Health Service Association, Tokyo, Japan; [f] Medical Science Institute Inc., Tokushima, Japan

ABSTRACT

Progression of thoracic aortic calcification (TAC) has been shown to be associated with hard cardiovascular events including stroke and all-cause mortality as well as coronary events. In this study, we propose an automated detection method of TACs of non-contrast CT images using mediastinal anatomical label map. This method consists of two steps: (1) the construction of a mediastinal anatomical label map, and (2) the detection of TACs using the intensity and the mediastinal anatomical label map. The proposed method was applied to two non-contrast CT image datasets: 24 cases of chronic thromboembolic pulmonary hypertension (CTEPH) and 100 non-CTEPH cases of low-dose CT screening. The method was compared with two-dimensional U-Nets and the Swin UNETR. The results showed that the method achieved significantly higher F1 score of 0.937 than other methods for the non-CTEPH case dataset (p-value < 0.05, pairwise Wilcoxon signed rank test with Bonferroni correction).

Keywords: Thoracic aorta calcification, computed tomography, anatomical label map

1. INTRODUCTION

Vascular calcification is linked to an increased risk of heart disease, stroke, and atherosclerotic plaque rupture [1][2]. Kälsch, et al. [2] investigated the association of thoracic aorta calcification(TAC)-progression with incident cardiovascular events and all-cause mortality in a population-based cohort and to determine its predictive value for these endpoints. They found that TAC progression is associated with hard coronary as well as cardiovascular events including stroke and all-cause mortality. Aortic calcified components can be quantified from non-contrast computed tomography (CT) by the Agatston method [3]. Automatic calcification scoring is expected that would enable routine cardiovascular risk prediction from low-dose chest CT scans. Various methods for vascular calcification detection and scoring from non-contrast CT images have been proposed [4]-[8], such as deep learning (DL)-based method for automatic calcium scoring across a wide range of CT examination types [6], and a convolutional neural networks (CNNs) to detect aortic calcifications and automate the TAC score assessment in intermediate cardiovascular disease risk patients [8].

Accurate recognition of mediastinal vascular and cardiac structures is one of the most important factors in the detection of TAC. Various methods for this task have been proposed [9]-[13]. Suzuki et al. proposed an accurate automatic segmentation method of the thoracic aorta and main pulmonary artery using an ensemble method of five U-Net architectures from non-contrast CT images [11]. Wasserthal et al. proposed the TotalSegmentator that is an automated segmentation method for multiple anatomical structures in whole body CT images, which demonstrated accurate segmentation results across a diverse dataset drawn from clinical routine [13]. In this study, we construct a mediastinal anatomical label map by combining three automated segmentation methods and use the map for detection of TACs. The overview of this framework is shown in Fig. 1. Its detection performance was evaluated by comparison with two-dimensional U-Net [14] and the Swin UNETR [15].

Medical Imaging 2023: Computer-Aided Diagnosis, edited by Khan M. Iftekharuddin, Weijie Chen, Proc. of SPIE Vol. 12465, 1246519 · © 2023 SPIE
1605-7422 · doi: 10.1117/12.2654043

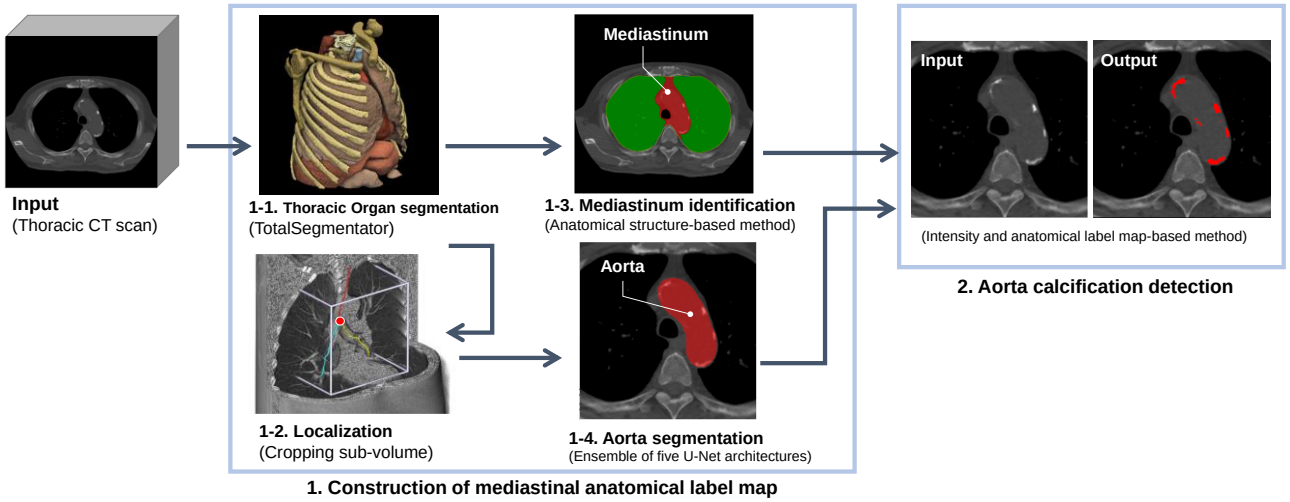

Fig. 1. Overview of the detection method of the aorta calcification using mediastinal anatomical label map.

2. MATERIALS AND METHODS

2.1 Non-contrast CT image datasets

This study used two datasets of non-contrast chest CT images: non-chronic thromboembolic pulmonary hypertension (non-CTEPH) cases of low-dose CT screening (dataset A) and CTEPH cases (dataset B). The collection and analysis of data were approved by the Institutional Review Board at Tokushima University. The CT images of dataset A were acquired on Aquilion Lightning scanner with 30 mA at 120 kVp, plane resolution: 0.625 mm, reconstruction matrix: 512 x 512, convolution kernel: FC01, slice thickness: 1.0 mm, and reconstruction interval: 1.0 mm. The CT images of dataset B were acquired on Aquilion ONE scanner with 112-295 mA at 120 kVp, plane resolution: 0.570-0.698 mm, reconstruction matrix: 512 × 512, convolution kernel: FC07, slice thickness: 0.5 mm, and reconstruction interval: 0.5 mm. The number of cases in datasets A and B was 100 and 24.

2.2 Manual annotation of thoracic aorta calcification

Examples of aorta and coronary artery calcifications in non-contrast CT images are shown in Fig. 2. The Agatston method [3] uses the weighted sum of lesions with a density above 130 HU, multiplying the area of calcium by a factor related to maximum plaque attenuation: 130-199 HU, factor 1; 200-299 HU, factor 2; 300-399 HU, factor 3; and ≥ 400 HU, factor 4. Based on this criterion, manual annotations of the TAC were performed using the CT value over 130 HU. The window level and width for the annotation were adjusted to 500 and 2000, respectively. The mean values and standard deviations of the calcium volume per scan for datasets A and B were 1,537.9 ± 1,960.7 mm^3 and 805.0 ± 889.2 mm^3, respectively. The histograms of the calcium volume per scan for datasets A and B are shown in Fig. 3.

2.3 Construction of mediastinal anatomical label map

The TotalSegmentator was applied to construct the basic anatomical label maps comprising of bone, airway, lungs, and heart. Then, the mediastinum region was identified by a segmentation method on the basis of the lungs and bone boundaries [16]. The aorta can also be segmented by the TotalSegmentator, however, accurate boundary recognition is required for the detection of the aorta calcification. Therefore, the aorta was segmented by a method comprised of the organ localization and an ensemble of five U-Net architectures [11]. In this process, a sub-volume centered on the tracheal bifurcation was cropped from original CT volume. The size of sub-volume is 256 × 256 × 256 pixels.

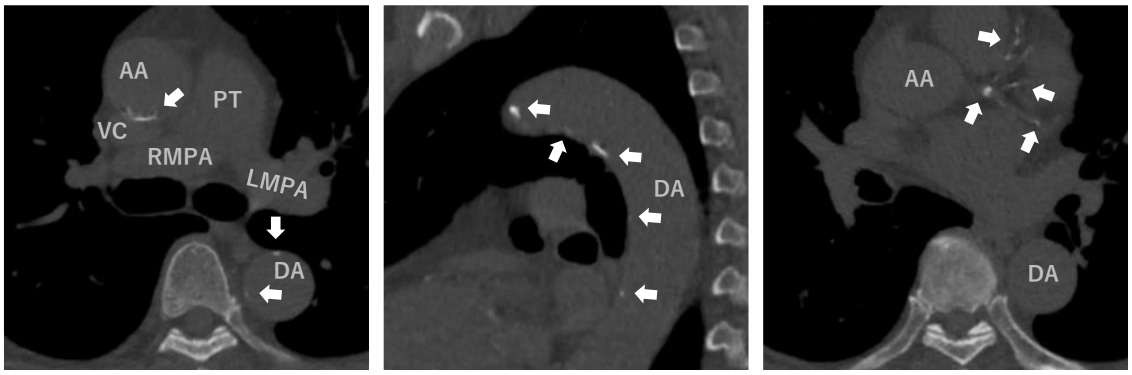

(a) (b) (c)

Fig. 2. Examples of aorta and coronary artery calcifications on non-contrast CT images. Aorta calcifications are shown in (a),(b), and coronary artery calcifications are shown in (c). AA, DA, VC, PT, RMPA, and LMPA are ascending aorta, descending aorta, vena cava, pulmonary trunk, right main pulmonary artery, and left main pulmonary artery. White arrows indicate the calcium regions.

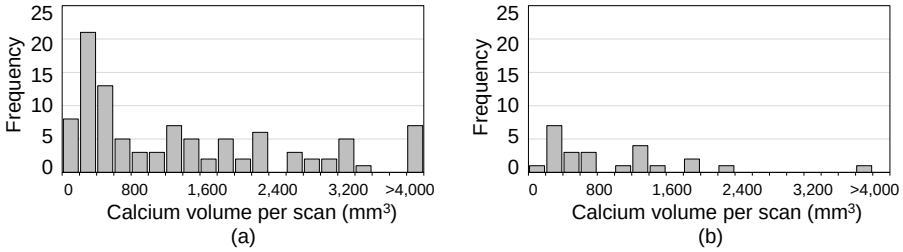

Fig. 3 Histograms of thoracic calcium volume per scan for datasets A (a) and B (b).

2.4 Detection of TACs using mediastinal anatomical label map

Low-dose CT images are noisy and this noise can cause CT values of exceeding 130 HU. This can lead to an increase in false positive results. Therefore, 3D bilateral filter [17] was adopted as the preprocessing. The spatial and range parameters were set to 1.5 and 30, respectively.

Initial seeds of the TAC were detected as pixels with CT value of over 130 HU in the aorta of the mediastinal anatomical label map. Then, the seeds within 5 mm from the aortic wall were adopted because calcifications occur near the aortic wall. These seeds were finally dilated using region growing to the regions over 130 HU within the mediastinum.

2.5 Evaluation of detection performance by comparison with the 2D U-Net architectures

The detection performance of TACs by the proposed method was compared with 2D U-Nets and the Swin UNETR. The training conditions of the methods are shown in Table 1. The axial slices for the training process were collected based on

Table 1 Training conditions of U-Nets and Swin UNETR.

Model	Dimension	Pre-trained model	Input size (pixel)	Optimization	Loss function	Mini-batch size	Epoch
U-Net	2D	No	256 × 256	Adam	Dice	4	40
U-Net (VGG-16)	2D	VGG-16 Encoder (ImageNet)	256 × 256	Adam	Dice	4	40
U-Net (patch-based)	2D	No	128 × 128	Adam	Dice	4	40
Swin UNETR	2D	No	256 × 256	Adam	Dice	4	40

two ways: (a) the sparse selection with the 10 slices interval, and (b) the selection of all slices including the ground truth regions. Training and testing were performed by 10-fold cross-validation using a mixed dataset of 100 non-CTEPH cases and 24 CTEPH cases. 5% of the training dataset was used for the validation dataset. The evaluation was performed in terms of three metrics: pixel-wise F1 score, pixel-wise sensitivity, and false positive volume per scan (mm^3). Pairwise comparisons were performed by Wilcoxon signed rank test with Bonferroni correction.

3. RESULTS

U-Nets were implemented using PyTorch [18] and MONAI framework [19] on a computer with a Core i9 central processing unit, 256 GByte memory, and NVIDIA RTX A6000 graphics processing units. The mean values and standard deviations of the metrics are shown in Table 2. In dataset A, the proposed method achieved the highest F1 score (p-value < 0.05). Among the DL-based methods, Swin UNETR achieved higher F1 score and sensitivity than the other DL-based methods (p-values < 0.05). In dataset B, the proposed method achieved high F1 score, however there were no significant difference in any of the metrics. Among the DL-based method, Swin UNETR achieved the higher sensitivity than other DL-based methods (p-value < 0.05). Examples of calcification detection results by the proposed method, U-Net, and Swin UNETR are shown in Fig. 4. The major false positives were observed at coronary artery bifurcations, near the esophagus and the bronchial wall.

Table 2 Detection performance of thoracic aorta calcifications for dataset A and B.

		F1 score	Sensitivity	False positive volume / scan (mm^3)
Dataset A	(A) Proposed method	0.937 ± 0.096*	0.940 ± 0.101	34.888 ± 58.202
	(B) U-Net	0.716 ± 0.293	0.659 ± 0.310	34.819 ± 71.314
	(C) U-Net (VGG-16)	0.848 ± 0.168	0.808 ± 0.197	34.464 ± 63.329
	(D) U-Net (Patch-based)	0.808 ± 0.215	0.903 ± 0.120	208.353 ± 300.745
	(E) Swin UNETR	0.898 ± 0.181	0.937 ± 0.148	68.856 ± 95.802
Dataset B	(A) Proposed method	0.894 ± 0.147	0.896 ± 0.145	10.996 ± 19.000
	(B) U-Net	0.790 ± 0.212	0.714 ± 0.266	23.860 ± 67.711
	(C) U-Net (VGG-16)	0.822 ± 0.254	0.803 ± 0.286	48.379 ± 124.249
	(D) U-Net (Patch-based)	0.654 ± 0.294	0.894 ± 0.116	474.564 ± 549.980
	(E) Swin UNETR	0.863 ± 0.239	0.961 ± 0.051	60.932 ± 94.771

(* p-value<0.05, pairwise Wilcoxon signed rank test adjusted by Bonferroni correction)

4. CONCLUSIONS

We presented an automated detection method of TACs from non-contrast CT images using a mediastinal anatomical label map. The proposed method achieved high detection performance of TACs with few false positives. The mediastinal anatomical label map would be useful to construct a simple, accurate, and evidence-explainable TAC scoring method.

REFERENCES

[1] Kälsch, H., Mahabadi, A. A., Moebus, S., Reinsch, N., Budde, T., Hoffmann, B., Stang, A, Jöckel, K., Erbel, R., Lehmann, N., "Association of progressive thoracic aortic calcification with future cardiovascular events and all-cause mortality: ability to improve risk prediction? Results of the Heinz Nixdorf Recall (HNR) study." European Heart Journal-Cardiovascular Imaging, 20(6), 709-717 (2019).

[2] Li, T., Yu, H., Zhang, D., Feng, T., Miao, M., Li, J., Liu, X., "Matrix vesicles as a therapeutic target for vascular calcification." Frontiers in Cell and Developmental Biology, 10, 25, (2022).

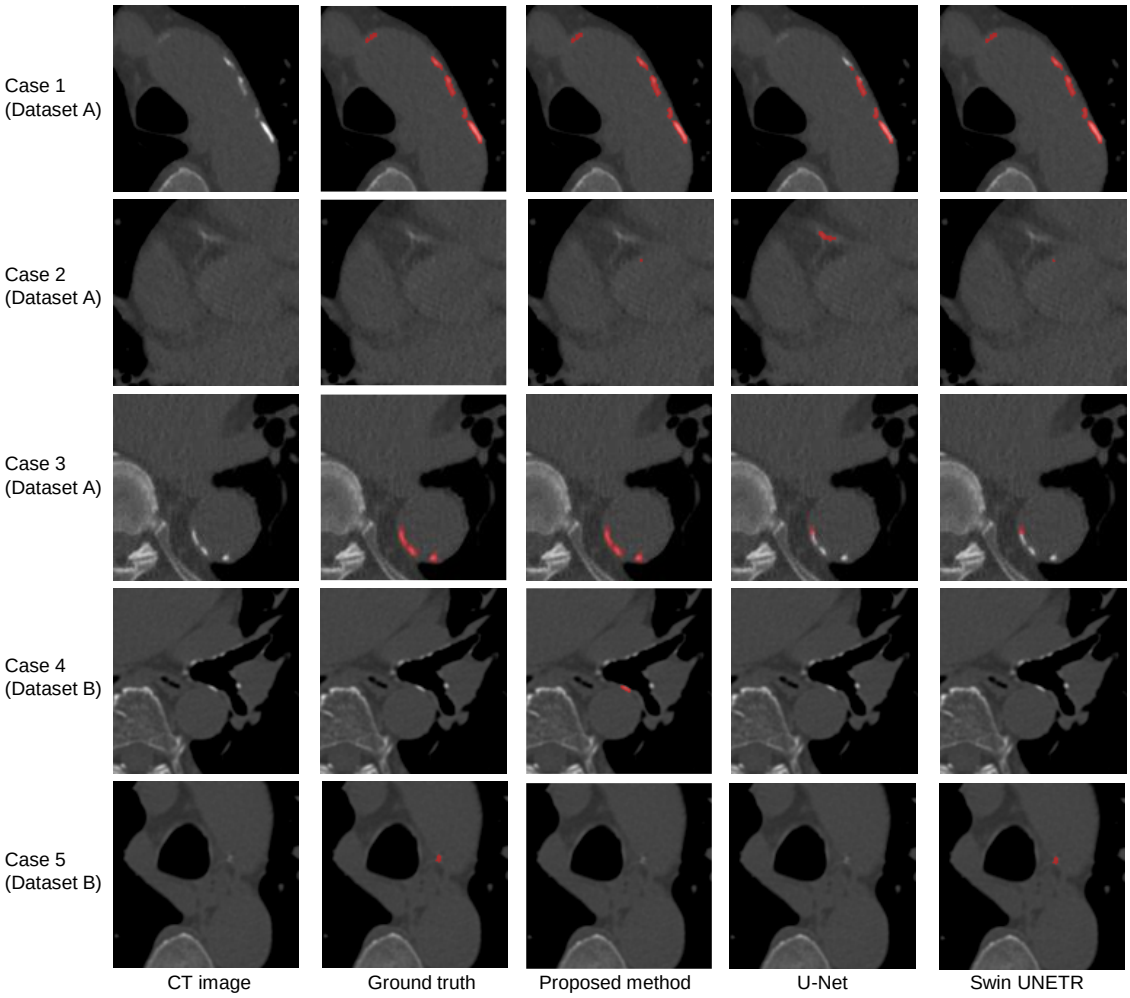

Fig. 4 Detection results of thoracic aorta calcifications by the proposed method, U-Net, and Swin UNETR.

[3] Agatston, A., S., Janowitz, W., R., Hildner, F., J., Zusmer, N., R., Viamonte, M., Detrano, R., "Quantification of coronary artery calcium using ultrafast computed tomography." Journal of the American College of Cardiology, 15(4), 827-832 (1990).

[4] Isgum, I., Prokop, M., Niemeijer, M., Viergever, M. A., Van Ginneken, B., "Automatic coronary calcium scoring in low-dose chest computed tomography." IEEE transactions on medical imaging, 31(12), 2322-2334 (2012).

[5] Wolterink, J. M., Leiner, T., de Vos, B. D., van Hamersvelt, R. W., Viergever, M. A., Išgum, I., "Automatic coronary artery calcium scoring in cardiac CT angiography using paired convolutional neural networks." Medical image analysis, 34, 123-136 (2016).

[6] Lessmann, N., van Ginneken, B., Zreik, M., de Jong, P. A., de Vos, B. D., Viergever, M. A., & Išgum, I., "Automatic calcium scoring in low-dose chest CT using deep neural networks with dilated convolutions." IEEE transactions on medical imaging, 37(2), 615-625 (2017).

[7] van Velzen, S. G., Lessmann, N., Velthuis, B. K., Bank, I. E., van den Bongard, D. H., Leiner, T., .de Jong, P., A., Veldhuis, W, B., Correa, A., Terry, J., G., Carr, J., J., Vergever, M., A., Verkooijen, H. M., Išgum, I., "Deep learning for automatic calcium scoring in CT: validation using multiple cardiac CT and chest CT protocols." Radiology, 295(1), 66-79 (2020).

[8] Guilenea, F., N., Casciaro, M., E., Pascaner, A., F., Soulat, G., Mousseaux, E., Craiem, D., "Thoracic Aorta Calcium Detection and Quantification Using Convolutional Neural Networks in a Large Cohort of Intermediate-Risk Patients." Tomography, 7(4), 636-649 (2021).
[9] Zhou, R., Liao, Z., Pan, T., Milgrom, S., A., Pinnix, C., C., Shi, A., Tang, L., Yang, J., Liu, Y., Gomez, D., Nguyen, Q., Dabaja, B., S., Court, L., Yang, J., "Cardiac atlas development and validation for automatic segmentation of cardiac substructures." Radiotherapy and Oncology, 122(1), 66-71 (2017).
[10] Morris, E., D., Ghanem, A., I., Dong, M., Pantelic, M., V., Walker, E., M., GlideHurst, C., K., "Cardiac substructure segmentation with deep learning for improved cardiac sparing." Medical physics, 47(2), 576-586 (2019).
[11] Suzuki, H., Matsuhiro, M., Kawata, Y., Niki N., Sugiura, T., Tanabe, N., Kusumoto, M., Eguchi, K., Kaneko, M., "Segmentation of aorta and main pulmonary artery of non-contrast CT images using U-Net for chronic thromboembolic pulmonary hypertension: evaluation of robustness to contacts with blood vessels" Medical Imaging 2022: Computer-Aided Diagnosis, 12033, 1203325 (2022).
[12] Pu, J., Leader, J., K., Sechrist, J., Beeche, C., A., Singh, J., P., Ocak, I., K., Risbano, M., G., "Automated identification of pulmonary arteries and veins depicted in non-contrast chest CT scans." Medical Image Analysis, 77, 102367 (2022).
[13] Wasserthal, J., Meyer, M., Breit, H. C., Cyriac, J., Yang, S., Segeroth, M., "TotalSegmentator: robust segmentation of 104 anatomical structures in CT images." arXiv preprint arXiv:2208.05868, (2022).
[14] Ronneberger, O., Fischer, P., Brox, T., "U-net: Convolutional networks for biomedical image segmentation," MICCAI 2015, 234-241 (2015).
[15] Tang, Y., Yang, D., Li, W., Roth, H., R., Landman, B., Xu, D., Nath, V., Hatamizadeh, A., "Self-supervised pre-training of swin transformers for 3d medical image analysis." Proceedings of the IEEE/CVF Conference on Computer Vision and Pattern Recognition, 20730-20740 (2022).
[16] Matsuhiro, M., Suzuki, H., Kawata, Y., Niki, N., Nakano, Y., Ohmatsu, H., Kusumoto, M., Tsuchida, T., Eguchi, K., Kaneko, M., "Peripleural lung disease detection based on multi-slice CT images." Medical Imaging 2015: Computer-Aided Diagnosis, 9414, 94142W (2015).
[17] Tomasi, C., Manduchi, R., "Bilateral filtering for gray and color images." Proc. Sixth Int. J. Conf. Computer Vision, 839-846 (1998).
[18] Paszke, A., Gross, S., Chintala, S., et al., "Automatic differentiation in pytorch." (2017).
[19] Cardoso, M. J., Li, W., Brown, R.,et al., "MONAI: An open-source framework for deep learning in healthcare." https://doi.org/https://doi.org/10.48550/arXiv.2211.02701 (2022).